FLUID INSTABILITIES IN RELATIVISTIC JETS. COMPARISON BETWEEN ANALYTICAL AND NUMERICAL APPROACHES.

M. Perucho[1,2], A.P. Lobanov[1] and J.M. Martí[2]

[1]Max-Planck-Institut für Radioastronomie, Bonn, Germany

[2]Universitat de València, Spain

Abstract

Relativistic outflows represent one of the best-suited tools to probe the physics of AGN. Numerical modelling of internal structure of the relativistic outflows on parsec scales provides important clues about the conditions and dynamics of the material in the immediate vicinity of the central black holes in AGN. We investigate possible causes of the structural patterns and regularities observed in the parsec-scale jet of the well-known quasar 3C 273. We present here the results from a 3D relativistic hydrodynamics numerical simulation in which we include jet precession and component injection. We compare the model with the structures observed in 3C 273 using very long baseline interferometry and constrain the basic properties of the flow. Our results show that matching accurately the model and observed structures requires smaller viewing angle of the jet than previously thought, thereby alleviating the constraints on the kinetic power and energy content of the jet.

Introduction

The relativistic jet observed in the quasar 3C273 is one-sided, with no signs of emission on the counter-jet side at dynamic ranges of up to 16,000:1. The enhanced emission features (jet components) identified in the jet on scales of up to ~20 milliarcseconds (mas) are moving at apparent speeds exceeding the speed of light by factors of 5-8. Plausible ranges of the Lorentz factor γ ~ 5-10 and viewing angles θ~10-15º have been inferred from these measurements. Ejections of new components into the jet occur roughly once every year (Krichbaum, Witzel, Zensus 2000). The position angle at which the components are ejected shows regular variations with a likely period of about 13-15 years (Abraham et al. 1996). These authors have suggested that this periodicity may reflect changes of the jet axis induced by the relativistic precession of the inner part of the accretion disk. Recent studies by Hardee (2000) have shown that the Kelvin-Helmholtz (K-H) instability may produce complex, three-dimensional ribbon-like and thread-like patterns inside a relativistic jet. In these ribbons and threads, a substantial increase of particle pressure and radio emissivity can be expected. The threaded structure forming a double helix has been detected in a space VLBI image of 3C 273 made at 5 GHz (Lobanov et al. 2000). It was explained in terms of K-H instability developing in a relativistic flow with modest Lorentz factor γ = 2.1 and relativistic Mach number M = 3.5 (Lobanov & Zensus 2001, hereafter LZ01). It is not clear whether the linear stability analysis can be still applied in the presence of these kind of non-linear effects in the flow. However, it is possible that jets preserve fingerprints of linear modes even when the non-linear regime features appear (Perucho et al. 2005). Numerical simulations should provide a means to address these problems by following the transition from linear to non-linear regimes of instability development (Perucho et al. 2004a,b). The ultimate goal of this work is to probe the advantages and limitations of combining the linear theory, numerical simulations and observations together, for the purpose of better understanding the physics of jets at parsec scales.

Linear analysis

LZ01 obtained 240 profiles of the brightness distribution across the jet. Profiles were centered on the ridge line of the jet, and orthogonal to it at each point. Then, a double gaussian was fit to each profile, and two components identified from the fit were interpreted as a double helix (see Fig. 1) caused by the action of K-H modes. They fitted wavelengths, phases and amplitudes of these modes. Approximations by Hardee (2000) to the characteristic wavelengths of a perturbed system, relate them to the speed of the jet (β_j), its Mach number (M_j) and the density ratio ($\eta=\rho_j/\rho_a$). Relating observed wavelengths to those parameters allowed LZ01 to derive the latter (see Table 1). We observe that the derived Lorentz factor is below those given by other authors in order to explain superluminal motion. However, this could possibly be caused by the fact that Kelvin-Helmholtz instability acts on the underlying, slower flow, and not on the ballistic, superluminal components (LZ01).

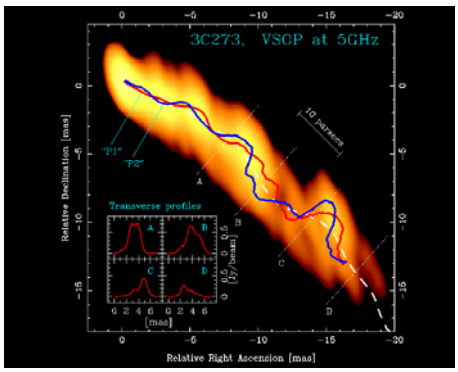

Figure 1. Double helix in the 3C 273 jet (LZ01). Dashed line identifies the ridge line of the jet. A, B, C, D mark the locations of the four profiles shown in the inset. The total of 240 profiles were measured in the jet and fit by two gaussians. The solid lines marked P1 and P2 show the locations of the peaks of the gaussians fitted.

γ_j	M_j	η	R_j(pc)	ϕ_j	θ_j	$c_{s,j}$ (c)	$c_{s,a}$ (c)	pc/mas
2.1	3.5	0.023	0.8	1.5	15	0.53	0.08	2.43

Table 1. Jet parameters from LZ01. γ_j is the jet Lorentz factor, M_j is the relativistic Mach Number, η is the density ratio, R_j is the jet initial radius, Φ_j is the jet half opening angle, θ_j is the angle to the line of sight, $c_{s,(j,a)}$ are the sound speeds in the jet and ambient medium, respectively, and the last column gives the projected parsecs per mas for 3C 273.

Numerical simulations

Numerical simulations have been performed with a 3D hydro-code. Initial setup consists on a steady jet with the parameters given in Table 1 and surrounded by a shear layer. Two different simulations were designed in order to explore the growth of K-H instabilities (simulation 3C273-A) and the effect of injected components and precession with observed frequencies (simulation 3C273-B) in a jet with those physical parameters.

Simulation 3C273-A

The numerical grid in this simulation is 211 R_j x 8 R_j, i.e., 169 pc x 6.4 pc. The axial size (169 pc) responds to the observed region by LZ01. Resolution is 16 cells/Rj in the transversal direction and 4 cells/R_j in the axial direction. Elliptical and helical modes are induced at the inlet. The frequencies of the excited modes are derived from the observed wavelengths, corrected for projection effects and relativistic motion, and wave speed, v_ω, given in LZ01 (v_ω=0.23c). Wavelengths found in simulations have to be related to those observed by means of the following relation:

$$\lambda^{theor} = \frac{\lambda^{obs}(1 - v_w/c\,\cos\theta)}{\sin\theta}, \qquad (1)$$

where λ^{theor} is the wavelength used, along with the corresponding wave speed, for deriving the driving frequencies of injected perturbations, λ^{obs} stands for the wavelength measured by the oserver, and θ is the angle to the line of sight (15º). This expression will also be used in order to extract the observed wavelengths from those found in the simulation.

The simulation can be divided in two parts, a first one, where modes grow linearly up to disruption of the jet, and a second part where disruption dominates evolution. Figure 2 shows transversal cuts at two different positions in the jet where the mode amplitudes are still linear (35 R_j and 105 R_j) and at three different times: this illustrates the rotation of structures in time and the way an elliptical (i.e., symmetric) mode dominates the jet structure closer to the injection and a helical (i.e., antisymmetric) mode dominates farther downstream, as stated in LZ01.

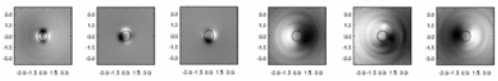

Figure 2. Transversal cuts at three different times in the jet at 35 Rj (three left panels) and 105 Rj (three right panels). The left panels illustrate the domination of the elliptical mode closer to the injection; the right panels illustrate the domination of hellical modes farther downstream.

In Fig. 3 we show an axial cut of pressure perturbation at R_j/2, in which antisymmetric (helical) λ~4 and λ~25 R_j modes and a symmetric (elliptic) λ~50 R_j mode can be identified. In Table 2 we show a comparison between the modes identified in LZ01 and those in the simulation depending on the wave speed of the mode. This speed could be measured for the helical λ~25R_j mode, from the motion of nonlinear structures close to the disruption point (v_ω~0.38c), and for the λ~50 Rj elliptic mode, from structure rotation similar to that observed in Fig. 2 (v_ω~0.2c, very close to the value reported in LZ01).

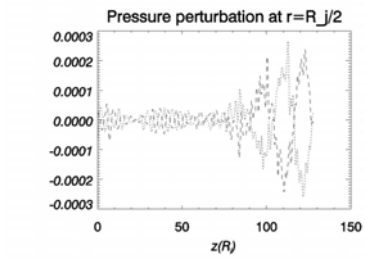

Figure 3. Axial cut of pressure perturbation at Rj/2 for the linear region of growth of the modes. We can identify three different structures: antisymmetric (helical) λ~4 (all through the cut) and λ~25 Rj (from 80 Rj) modes and a symmetric (elliptic) λ~50 Rj (up to 80 Rj) mode. Dashed and dotted lines stand for symmetric points around the jet axis.

λ^{obs} (mas)	Mode	λ^{theor} (R_j)	λ^{sim} (R_j)	$\lambda^{sim}_{v_w=0.23c}$ (mas)	$\lambda^{sim}_{v_w=0.38c}$ (mas)	$\lambda^{sim}_{v_w=0.88c}$ (mas)
2	H_{b2}	18.7	4	0.44	0.54	2.27
4	E_{b1}, H_{b1}	37.4	25	2.7	3.37	14.3
12	E_s	21.2[a]	50	5.5	6.7	28.5

Table 2. First two columns give identified wavelengths and modes in LZ01 (*H* stands for helical, *E* for elliptical, *s* for surface mode and *b1* and *b2* for first and second body modes, respectively), third column gives the intrinsic wavelengths (see text), in the fourth column we have written measured wavelengths in the simulation, and the last three columns give the fourth column wavelengths as observed depending on the wave speed, derived with Equation (1). First wave speed is that from the fits in LZ01, second is that measured in the simulation for the 25 Rj helical mode and third is the flow speed. Superscript *a* stands for computed assuming it propagates with the flow speed.

Table 2 illustrates the correspondance between the simulated and observed structures, depending on the wave speed. It is remarkable that, with the measured wave speeds for the helical λ~25 Rj and the elliptical λ~50 R_j modes, we obtain close results to wavelengths given in LZ01 (3.37 mas vs 4 mas, 5.5 mas vs 4 mas). Why we don't see the other modes is to be studied. The longest mode, with the wave speed given in LZ01, would require a 150 R_j wavelength in the simulation, which is difficult to observe even in a grid as large as was used here, in particular when shorter harmonics grow fast and disrupt the flow.

Simulation 3C273-B

In this second simulation we try to study the effect of precession and injection of fast components on the observed structures in the jet. The precession frequency is given by the observed 15 yr periodicity of position angle variations (Abraham et al. 1996). The frequency of ejections of components is set by the reported 1 yr periodicity (Krichbaum et al. 2000). The duration of each ejection is estimated to be 2 months, from the approximate inspiralling time from an orbit at ~6 R_G around a 5.5 10^8 solar mass black hole. Velocity of the components is taken as constant with the mean value of those given by Abraham et al. (1996), i.e., Lorentz factor γ~5. The components are treated as shells of diameter 0.5 R_j ejected, in a centered position with respect to the axis. The numerical grid for this simulation covers 30 R_j (axial) x 6 R_j (transversal), i.e., 24 pc x 4.8 pc. The resolution of the grid is 16 cells/R_j in both transversal directions and 32 cells/R_j in the direction of the flow.

In Figure 4 we show axial cuts of pressure perturbation close to the jet axis and at the jet radius. We observe two typical wavelengths: a symmetric one (λ~0.4 R_j), dominating close to injection, and an antisymmetric one (λ~4 R_j). The first is clearly observed close to the jet axis, and also after z~3-4 R_j in the boundaries, whereas the latter dominates on the boundaries, close to injection, and the overall structure since z~10 R_j, modulated by short wavelength close to the axis. The amplitudes of the injected fast components decreases outwards (see Fig. 5), in agreement with the result by Lobanov and Zensus (1999) and Lobanov and Roland (2001), who claim that relativistic shocks should dominate emission at small scales but are likely to dissipate at distances larger than ~10 pc, and that they share importance with instabilities from ~10 to ~100 pc. This effect could be caused by numerical diffusion due to the low resolution used in the simulation. However, the strong peaks observed in the antisymmetric structure in Fig. 4 are related with the drift of components towards outer radial positions of the jet, similar to that reported by LZ01.

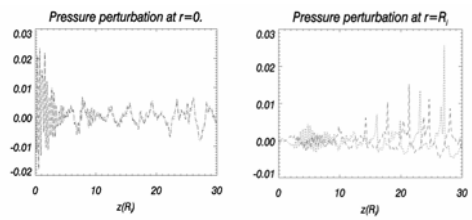

Figure 4. Axial cuts of pressure perturbation at r~±1/16 R_j (left) and at r~±Rj (right).

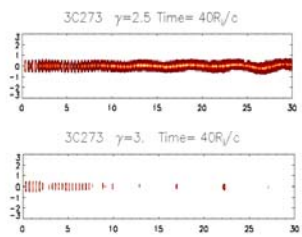

Figure 5. Surface plots for Lorentz factors 2.5 and 3.

Table 3 is the equivalent version of Table 2 for the present simulation. We can see that the derived wavelengths are far too small to be comparable with the 2-4 mas elliptic modes (for the symmetric structure) or with the 18 mas mode (for the antisymmetric structure), interpreted by LZ01 as due caused by precession. From Equation (1) we deduce that smaller angles to the line of sight and higher component velocities would be needed in order to reproduce them. Recent observations by Jorstad et al. (2005) allow them to derive a viewing angle of 6º to the jet in 3C 273, and component Lorentz factors of aroun 10, which would give 1.4 mas and 14 mas for the symmetric and antisymmetric waves in our simulation. These values are much closer to those reported by LZ01 and would confirm our hypothesis.

λ^{sim} (R_j)	$\lambda^{sim}_{v_w=0.88\,c}$(mas)	$\lambda^{sim}_{v_w=0.94\,c}$(mas)	$\lambda^{sim}_{v_w=0.98\,c}$(mas)
0.4 (symmetric)	0.23	0.37	0.62
4 (antisymmetric)	2.27	3.7	6.2

Table 3. In the first column we have written measured wavelengths in the simulation, and the last three columns give the fourth column wavelengths as observed depending on the wave speed, derived with Equation (1). First wave speed is that of the underlying flow, second is that for the fastest modes propagating downstream (see Fig. 6) and third is the component injection speed.

Main conclusion of simulation 3C273-B is that nonlinear features as relativistic shocks or black hole precession may produce linear structures and couple to K-H modes, as shown by the spatial growth of the helical structure).

Conclusions

We have shown that numerical simulations may be used to constrain basic parameters of the jets as speed or viewing angles. The inclusion of magnetic fields (see Asada et al. 2002), decreasing density atmospheres and relativistic equation of state in simulations, along with high resolution observations will allow us to reconstruct, in much better detail, physical conditions in real extragalactic jets.

Bibliography

Abraham, Z. et al., 1996, A&AS, 115, 543
Asada, K., et al., 2002, PASJ, 54, L39
Hardee, P.E., 2000, ApJ, 533,176
Jorstad,S.G. et al., 2005, AJ, in press
Krichbaum, T. et al., 2000, Proc. 5th EVN Symposium.
Lobanov, A.P., Zensus, J.A., 1999, ApJ, 521, 509
Lobanov, A.P., Roland, J., 2001, ASP Conference Proceedings, v.250, 195
Lobanov, A.P., Zensus, J.A., 2001, Science, 294, 128 (LZ01)
Lobanov, A.P. et al., 2000, Advances in Space Research, 26, 669
Perucho, M. et al., 2004a, A&A, 427, 415
Perucho, M. et al., 2004b, A&A, 427, 431
Perucho, M. et al., 2005, A&A, in press